Nanoscale

Accepted Manuscript

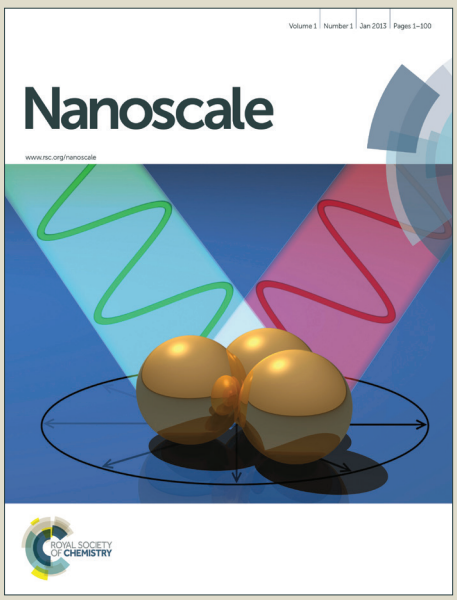

ROYAL SOCIETY OF CHEMISTRY

www.rsc.org/nanoscale

Concurrent Ordering and Phase Transformation in $SmCo_7$ Nanograins

Martin Seyring[1,*], *Xiaoyan Song*[2,*], *Zhexu Zhang*[2], *Markus Rettenmayr*[1]

1. Otto Schott Institute of Materials Science, Friedrich Schiller University, D-07743 Jena, Germany
2. College of Materials Science and Engineering, Key Laboratory of Advanced Functional Materials, Ministry of Education of China, Beijing University of Technology, Beijing 100124, P. R. China

*Corresponding authors:
Dr. Martin Seyring
email: martin.seyring@uni-jena.de
Prof. Xiaoyan Song
email: xysong@bjut.edu.cn

Abstract

Sm-Co alloys with stabilized $SmCo_7$ phase are most prominent candidates for advanced high temperature permanent magnets, where the stabilization of the $SmCo_7$ phase can be effectuated by nanostructuring. The complex concurrent processes of ordering and phase transformation in a $SmCo_7$ nanograin are characterized on the atomic scale. For the first time early stages of the phase transformation are made visible by highlighting specific superstructures in single nanograins using Fourier reconstruction of high-resolution transmission electron microscopy images. The superstructures are only detectable and can only be distinguished in specific crystallographic orientations. The evolution of the atom arrangement in the crystal structures is demonstrated for the concurrent ordering process and phase transformation. During decomposition of the metastable $SmCo_7$ phase, the hexagonal Sm_2Co_{17} superstructure (2:17H) forms at first as precursor of the rhombohedral Sm_2Co_{17} superstructure (2:17R) – this can only be detected by analysis of individual grains and has not been described so far. By extensive crystallographic analysis of individual nanograins, a distinct correlation between the fraction of the superstructure phases and the grain size is found, showing directly and unambiguously the grain size dependence of the phase

transformation in the nanocrystalline alloy, a phenomenon that so far was only shown indirectly using volume averaging methods.

.

Keywords: nanocrystalline materials, phase transformation, order-disorder transformation, superstructure, transmission electron microscopy, $SmCo_7$ alloys

1. Introduction

Sm-Co intermetallic compounds are known to be the best performing permanent magnets in the high temperature range.[1-3] Compared with the equilibrium phases Sm_2Co_{17} (2:17) and $SmCo_5$ (1:5), the metastable phase $SmCo_7$ (1:7) offers higher Curie temperature together with strong uniaxial magnetocrystalline anisotropy.[4] Thus, alloys with stabilized 1:7 phase are the prime candidates for advanced permanent magnets that are to be applied in the high temperature range.[5, 6] In conventional polycrystalline Sm-Co alloys, the 1:7 phase with a $TbCu_7$-type structure does not exist, but decomposes to Sm_2Co_{17} with a Th_2Zn_{17}-type structure (2:17R) and 1:5.[7, 8] A well-known method that is documented in the literature in several instances is doping by a third element (e.g. Si, Cu, Ga, Nb, Zr, Ti, Hf) to stabilize the metastable 1:7-phase.[4, 9, 10] However, in nanocrystalline alloys the 1:7 phase stability is significantly changed [11, 12] owing to the high grain boundary fraction and the resulting change in the Gibbs free energy, which in turn affects the phase transformation behavior. Particularly the stability of the 1:7 phase is enhanced by nanostructuring.[13, 14] To improve on the one hand the hard magnetic performance by tailoring the microstructure, and to increase on the other hand the maximum service temperature and the lifetime at elevated temperatures, detailed studies on the phase stability and transformation mechanisms in nanocrystalline $SmCo_7$ are a prerequisite. Although in our previous work the decomposition of the 1:7 phase at

temperatures above 600°C was reported and thermodynamic calculations of the critical grain size for phase destabilization were performed,[13, 15] the phase transformation mechanism within single nanograins, particularly the ordering process of the 1:7 crystal structure at the atomic scale, are essentially unknown.

It is important to note that in the X-ray diffraction (XRD) patterns, the 1:7 and 2:17 crystal structures only differ by the occurrence and position of superstructure reflections with low intensity,[16, 17] which can hardly be resolved at low volume fractions. Peak broadening in the nanocrystalline alloys further aggravates a reliable phase detection and quantification of phase fractions. In this respect, electron diffraction in the transmission electron microscope (TEM) provides a much higher signal to noise ratio[18] and hence a higher sensitivity for analyzing nanocrystals.[19] Thus, by TEM characterization and extended diffraction analysis, initial stages of the phase destabilization in nanocrystalline 1:7 are accessible. Seeing that there is an impact of the grain size on the phase stability, also the ordering process in magnetic nanomaterials should be affected by the grain length scale.[20, 21] In the present paper, the ordering and phase transformation processes of the 1:7 structure within single nanograins are studied in detail by means of crystallographic analysis with the highest possible resolution using high resolution TEM (HRTEM) and nanobeam electron diffraction (NBED).

2. Results and Discussion

Figure 1 shows the microstructures and the azimuthal integrated SAED profiles[18] of the nanocrystalline $SmCo_7$ samples for the as-prepared and annealed (600°C and 700°C for 0.5h, respectively) states. Annealing of the as-prepared nanocrystalline $SmCo_7$ alloy causes grain coarsening that is accompanied by a phase transformation from the disordered 1:7 phase to the ordered 2:17R phase. In the as-prepared sample with a mean grain size of ~21nm (Figure 1b), only the principal reflections of the disordered 1:7 phase are visible in the SAED profile (Figure 1a). For the sample annealed at 600°C for 0.5h with the mean grain size increasing to

~35nm (Figure 1c), weak superstructure reflections appear in the SAED profile (indicated by arrows in Figure 1a), which implies the onset of the ordering transformation. In the sample annealed at 700°C for 0.5h, the mean grain size has increased to ~161nm (Figure 1d).

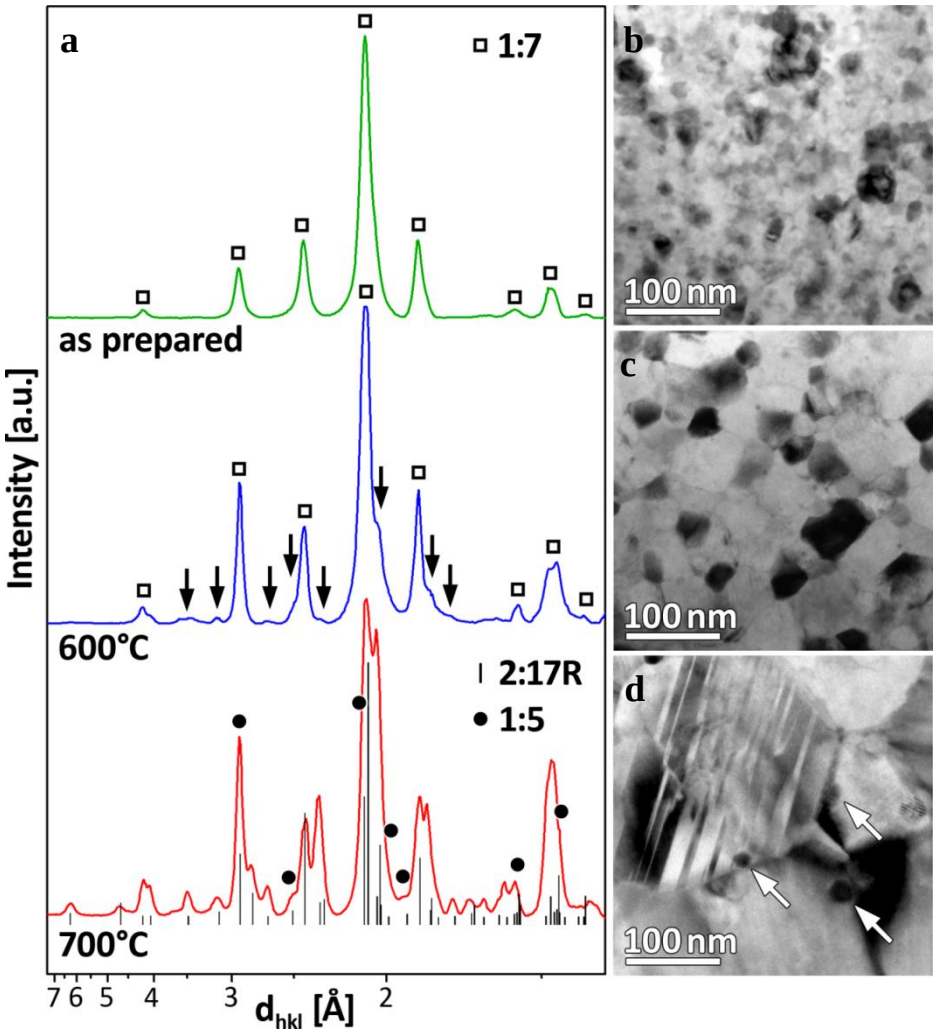

Figure 1. Microstructures and corresponding diffraction patterns of the nanocrystalline $SmCo_7$ samples at different states: (a) azimuthal integrated SAED profiles; (b) TEM image of the as-prepared sample; (c) TEM image of the sample annealed at 600°C for 0.5h; (d) TEM image of the sample annealed at 700°C for 0.5h. The arrows indicate weak superstructure reflections (a) and precipitates (d), respectively.

The corresponding SAED profile (Figure 1a) shows pronounced superstructure reflections that match with the theoretical peak positions of the rhombohedral 2:17R phase (indicated by black lines in Figure 1a). There is discrepancy to the theoretical intensity distribution, which is due to the crystallographic texture that in turn is a consequence of the formation of anti-

phase domains during the ordering process.[21] The sharp diffraction contrast of the upper left grain in Figure 1d) reveals such anti-phase domain structure. The ordering transformation is accompanied by the precipitation of the 1:5 phase, since the formation of 2:17R requires a somewhat higher Co concentration than that in the initial 1:7 phase. The precipitates at grain and domain boundaries (indicated by arrows in Figure 1d) have already been identified as 1:5 phase by combining HRTEM and NBED analysis in our previous work.[15]

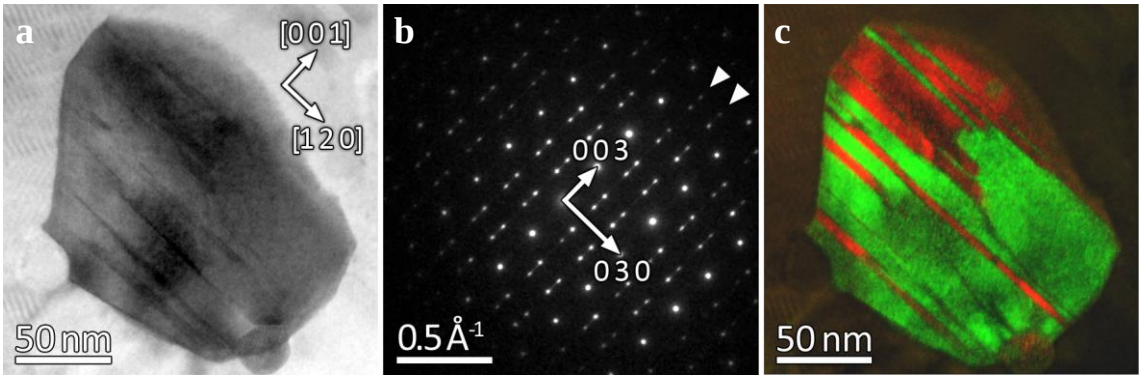

Figure 2. Diffraction analysis and superposed dark field images of a grain in $[1\,0\,0]_{2:17R}$ orientation in the sample annealed at 700°C for 0.5h: (a) bright field image; (b) corresponding SAED pattern and indexing, triangles indicating the superstructure reflections of the 2:17R phase; (c) dark field image generated by the superposition of the superstructure reflections of the two twin variants (displayed as red and green), showing that the whole grain contains only 2:17R phase.

It is found that the ordering process in the nanocrystalline $SmCo_7$ is completed in the sample annealed at 700°C for 0.5h. As an example, the characterization of a single grain in this sample is shown in Figure 2. The size of the grain is measured as 166nm, which is very close to the mean grain size. The corresponding SAED pattern contains superstructure reflections of the 2:17R phase, as indicated by the triangles in Figure 2b). Two dark field images using by the twin variants of the superstructure reflections in Figure 2b) are combined in Figure 2c), one of the dark field images displayed in green, the other one in red color. A comparison of Figure 2a) and Figure 2c) confirms that the two variants of the superstructure reflections reproduce the entire projected area of the grain. Thus, the combined SAED pattern

and dark field image analysis indicate the completion of the phase transformation from 1:7 to 2:17R in this grain.

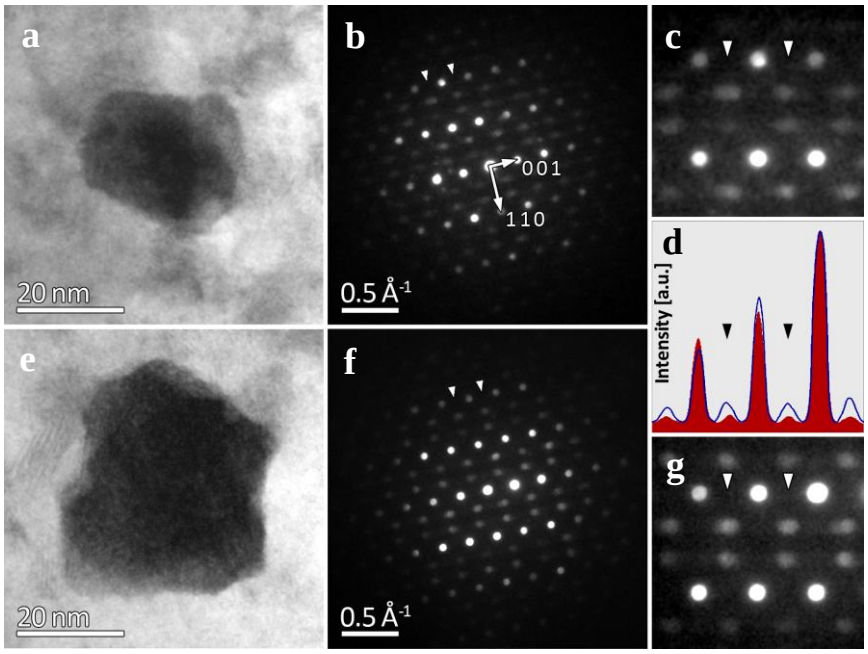

Figure 3. Appearance of superstructure reflections of 2:17H in the $[1\text{-}1\ 0]_{1:7}$ orientation in the as-prepared sample in nanograins with different sizes: (a, e) bright field images of nanograins with sizes of 30 and 44nm, respectively; (b, f) corresponding NBED patterns; (c, g) local enlargement of the superstructure reflections; (d) intensity profiles integrated along $(110)_{1:7}$ over 8 superstructure reflections corresponding to the grains of 30nm (red) and 44nm (blue). The triangles indicate the typical superstructure reflections of the 2:17H phase.

In the as-prepared sample with the finest grain structure, the nanograins with sizes above 30nm contain a small fraction of the hexagonal Th_2Ni_{17}-type (2:17H) structure. The overall fraction of the 2:17H phase in this sample is below 5%. Due to its low phase fraction, its local appearance and the relationship between the lattice structures of all involved phases, 2:17H cannot be detected by conventional XRD analysis. As shown in Figure 3, the crystallographic analysis of nanograins with NBED indicates that the phase fraction of 2:17H is dependent on the size of the corresponding grain. The two grains in Figure 3a) and e) have sizes of 30 and 44nm, respectively. Their corresponding NBED patterns in the $[1\text{-}1\ 0]_{1:7}$ orientation show specific superstructure reflections of 2:17H (indicated by triangles in Figure 3b) and f). The arrows in Figure 3b) represent the reciprocal lattice vectors. In the local enlargement of the NBED patterns (Figure 3c and g), the superstructure reflections appear sharper for the larger

grain as compared to that of the smaller grain. As more clearly seen in the profiles exhibiting the integrated intensity along $(1\ 1\ 0)_{1:7}$ over 8 superstructure and 4 principal reflections (Figure 3d), the intensity of the superstructure reflections is clearly higher for the larger grain (blue line, see Figure 3d), demonstrating the grain size dependence of the transformation of the 2:17H superstructure from the 1:7 matrix.

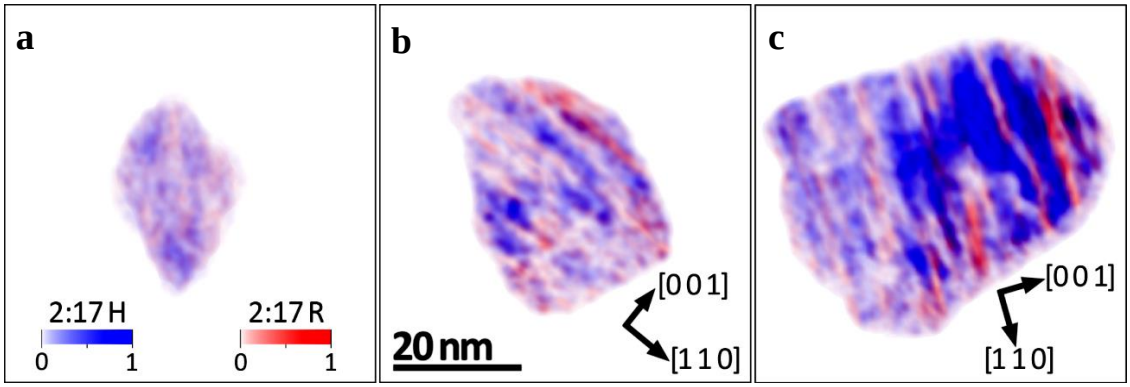

Figure 4. Highlighted superstructure regions in nanograins with different sizes in the sample annealed at 600°C for 24h: (a) grain size 25nm; (b) 38nm; (c) 49nm. The amplitude images are generated by Fourier reconstruction and accentuated by gamma correction. The intensity scales in (a) are normalized to the amplitudes of the principal reflections.

For a better insight in the mechanism of the 1:7 phase transformation, the occurrence of the superstructure in single nanograins was analyzed in more detail by highlighting the superstructure regions in HRTEM micrographs using Fourier reconstruction. The theoretical basis of this method can be found in the literature.[22-24] In the nanograin, for all regions occupied by 2:17H and 2:17R phase, all unique superstructure reflections (Fourier components) were selected in the Fourier spectrum to generate an amplitude image corresponding to their lattice fringes in the HRTEM micrograph. The resultant amplitude image highlights the superstructure phase. Figure 4 shows the distribution of 2:17H and 2:17R superstructure phases in single nanograins by their amplitude images. Grains with different sizes were chosen in the sample annealed at 600°C for 24h. The grain with a size of 25nm contains weak amplitude signals of the 2:17H superstructure (blue in Figure 4a). A distinct amplitude signal of the 2:17R superstructure is not visible. In the grain with a size of 38nm

(Figure 4b), both the 2:17H and 2:17R superstructure regions are present, and regions of the 2:17R phase adjoin to those of the 2:17H phase. In the grain with a size of 49nm (Figure 4c), strong amplitudes of the 2:17H and 2:17R superstructures are visible. Moreover, the 2:17H and 2:17R regions develop alternatively in the nanograin. It is found in all the analyzed nanograins that the 2:17R phase forms inside or adjacent to the 2:17H region. The 2:17R phase has a plate-like morphology and is stacked along the *c*-axis of the grain.

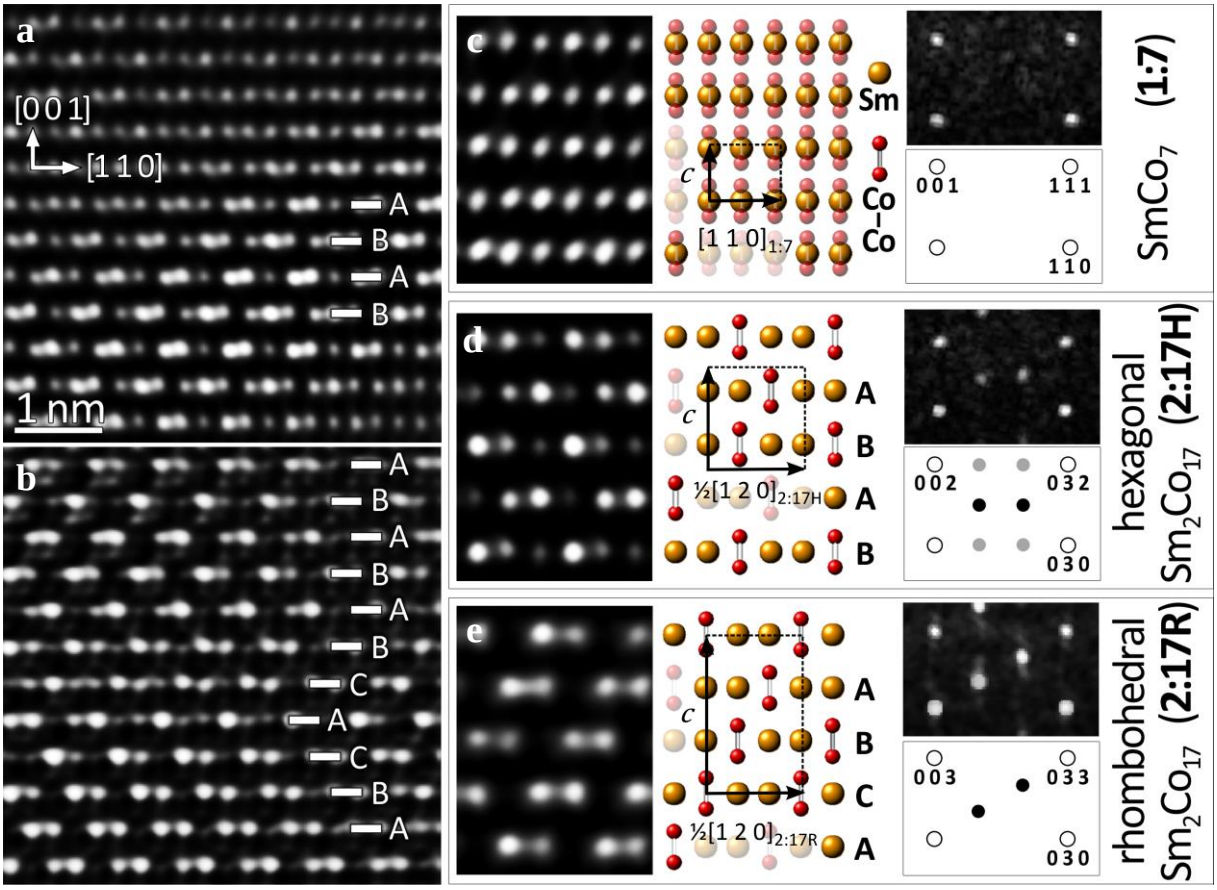

Figure 5. Evolution of the atomic arrangement during the concurrent ordering and phase transformation: (a) HRTEM image at the phase boundary between 1:7 (upper part) and 2:17H (lower part); (b) HRTEM image at the phase boundary between 2:17H (upper part) and 2:17R (lower part); (c-e) representative HRTEM images, corresponding projected crystal structures and Fourier diffractograms in comparison with the theoretical reflection positions for 1:7, 2:17H and 2:17R phases, respectively. A, B and C indicate the stacking sequence of atomic layers.

Details of the crystal structures during the concurrent processes of ordering and phase transformation from 1:7 to 2:17R are shown in Figure 5, demonstrated by the change in the characteristic atomic arrangement. The HRTEM image at the phase boundary between 1:7

and 2:17H in a 44nm grain at the initial state (Figure 5a), together with the Fourier diffractograms and schematic representation of the crystal structures projected (Figure 5c and d), reveals the ordering process from 1:7 to 2:17H. The order or disorder state is attributed to the degree of the periodic arrangement of the Co-Co dumbbells in the lattice.[17] In the 1:7 phase, the Co-Co dumbbells are located randomly on the suitable lattice sites.[7] Due to their random distribution, the relevant atom columns appear with uniform grey shade (Figure 5c). The ordering occurs by alignment of the Co-Co dumbbells in specific atom columns with respect to Sm atoms, leading to an ordered stacking sequence ABAB... (indicated in Figure 5a and d).[25, 26] The ordering of 1:7 results in the 2:17H superstructure. Further, the HRTEM image of a 58nm grain after annealing at 600°C for 30min displays the phase boundary between 2:17H and 2:17R (Figure 5b). The change in the location of Co-Co dumbbells with respect to the Sm atoms in the 2:17H superstructure causes a different configuration in the lattice, and hence a differently ordered stacking sequence, particularly ABCABC... (marked in Figure 5b and shown by the atomic arrangement in Figure 5e).[25, 26] The 2:17R superstructure forms at the border of 2:17H. As compared with the crystal structure of 2:17R, the 2:17H superstructure has a higher symmetry and a simpler atomic arrangement concerning the Co-Co dumbbells, and can form more easily from the disordered 1:7 matrix. The ordering process of 1:7 to 2:17H is a discontinuous first-order transformation,[27] leading to the coexistence of 1:7 and 2:17H in the nanograin. Subsequently, 2:17R forms from 2:17H. Thus, the 2:17H superstructure acts as the precursor of the 2:17R equilibrium phase.

As observed from the TEM micrographs, in the nanograins where the ordering transformation of the 1:7 phase is initiated, the 2:17H exists mainly in smaller grains, while the 2:17R is found generally in larger grains. To quantify the influence of grain size on the phase transformation in the 1:7 matrix, the fractions of the 2:17H and 2:17R phases were determined from the amplitude images by binarization. Considering that the completion of phase transformation from 1:7 to 2:17R in larger grains is already clearly shown in Figure 1

and Figure 2, only smaller grains with a size below 60nm were analyzed as to gain access to the early stages in the process of ordering transformation and formation of 2:17R. Larger grains whose sizes distinctly exceed the thickness of the TEM foil may in addition be influenced by the different environment (no stabilizing grain boundaries above and below the grain of interest, surface energy influence) and were not analyzed.

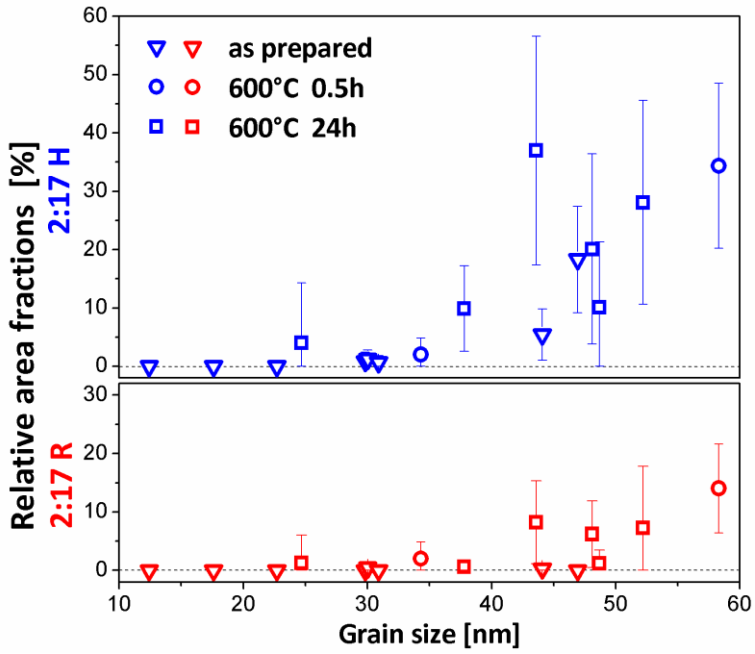

Figure 6. Fractions of the superstructure phases as a function of grain size for nanocrystalline samples at different states.

Figure 6 shows the relative area fractions of the 2:17H and 2:17R phases as a function of the grain size. The data points represent the mean value measured from at least 10 HRTEM images per grain, depending on the grain size. Independent of the state of the samples, all measurements indicate a similar relationship between the phase fractions and the grain size. In grains with sizes below 25nm, no fraction of 2:17H or 2:17R phase has been detected. Significant fractions of the 2:17H phase are only observed for grain sizes above 40nm. The quantitative characterization in Figure 6 demonstrates the grain size dependence of the 1:7 phase transformation, and confirms that 2:17H forms earlier than 2:17R. The statistic results are consistent with the thermodynamic calculations on the phase stability in the nanocrystalline $SmCo_7$ alloy. [14, 28, 29] Thermodynamic calculations predict that due to the

reduction of the Gibbs free energy of the nanocrystalline alloy system, the 1:7 phase decomposes to 2:17R and 1:5 phases at grain sizes above a critical value of ~50nm.

3. Conclusion

In summary, the detailed investigations combining HRTEM and NBED analysis give clear insight into the concurrent ordering and phase transformation processes in the nanocrystalline $SmCo_7$ alloy at the atomic scale. By highlighting the superstructures from the HRTEM images of several single nanograins with Fourier reconstruction, early stages of the phase transformation are visualized for the first time in the microstructure. This solved the long-standing problem that the characteristics of 1:7 ordering could not be resolved or even detected by the XRD.[16, 17] We further identified for the first time that 2:17H is the precursor of 2:17R during the phase transformation $SmCo_7 \rightarrow Sm_2Co_{17} + SmCo_5$.

The effects of grain size on the occurrence of 2:17H and 2:17R superstructures were demonstrated by both crystallographic analysis on atomic arrangement within individual nanograins and a statistic study on the correlation between the phase fraction and nanograin size. The identified mechanism shows directly the grain size dependence of the concurrent ordering and phase transformation of 1:7 $\rightarrow$ 2:17H $\rightarrow$ 2:17R. The concept of a critical grain size for the phase transformation[28, 30, 31] is experimentally confirmed with our high resolution study. The method in the present work is applicable for the characterization of nanoscale phase stability in various alloy systems, and our findings facilitate the structural control of nanocrystalline materials. To further extend the stability of the 1:7 phase to temperatures above 600°C combining nanostructuring and doping with a third element[9, 10] appears to be an appropriate means.

4. Experimental

Fully dense, single phase $SmCo_7$ nanocrystalline bulk material was prepared using a recently developed route, starting from a cast ingot with the stoichiometric composition, using ball milling to produce amorphous powder, and performing spark plasma sintering to densify to a bulk compound with a mean grain size of about ~21nm. The detailed processing procedures are presented in our previous work.[15] The as-prepared nanocrystalline $SmCo_7$ bulk was sectioned into a series of samples and annealed in a vacuum furnace at 600°C and 700°C, respectively, in a time range from 0.5h to 24h. The samples were examined in a JEOL 3010HT TEM equipped with a high-resolution pole piece and a LaB_6 cathode and operating at 300kV. As a measure for the grain size we use the area equivalent circular diameter. High resolution TEM (HRTEM), nanobeam electron diffraction (NBED) and selected area electron diffraction (SAED) were applied for the crystallographic characterization of the nanocrystalline structure. Diffraction analysis of single nanograins was performed by NBED, allowing a spatial resolution of <5nm.[20, 32] Fourier reconstruction of the HRTEM image was used to highlight the superstructure and evaluate the phase fractions in nanograins.

Acknowledgements

X. Song thanks the financial support from the National Natural Science Foundation of China (51371012). All the authors gratefully acknowledge the financial support by German Science Foundation (DFG) (Grant Re1261/9 and SO 1075/1-2).

References

1. K. H. J. Buschow, *Reports on Progress in Physics*, 1991, **54**, 1123-1213.
2. Y. L. Hou, Z. C. Xu, S. Peng, C. B. Rong, J. P. Liu and S. H. Sun, *Adv. Mater.*, 2007, **19**, 3349-+.
3. Z. X. Zhang, X. Y. Song, Y. K. Qiao, W. W. Xu, J. X. Zhang, M. Seyring and M. Rettenmayr, *Nanoscale*, 2013, **5**, 2279-2284.
4. Y. Q. Guo, W. Li, W. C. Feng, J. Luo, J. K. Liang, Q. J. He and X. J. Yu, *Appl. Phys. Lett.*, 2005, **86**, 3.

5. I. A. Al-Omari, Y. Yeshurun, J. Zhou and D. J. Sellmyer, *Journal of Applied Physics*, 2000, **87**, 6710-6712.
6. J. Zhou, I. A. Al-Omari, J. P. Liu and D. J. Sellmyer, *Journal of Applied Physics*, 2000, **87**, 5299-5301.
7. Z. D. Zhang, W. Liu, J. P. Liu and D. J. Sellmyer, *Journal of Physics D-Applied Physics*, 2000, **33**, R217-R246.
8. S. Reutzel, J. Strohmenger, T. Volkmann, J. Gao and D. M. Herlach, *Mater. Sci. Eng. A-Struct. Mater. Prop. Microstruct. Process.*, 2007, **449**, 709-712.
9. J. Luo, J. K. Liang, Y. Q. Guo, Q. L. Liu, F. S. Liu, Y. Zhang, L. T. Yang and G. H. Rao, *Intermetallics*, 2005, **13**, 710-716.
10. M. J. Dospial, M. G. Nabialek, M. Szota, T. Mydlarz, K. Ozga and S. Lesz, *J. Alloy. Compd.*, 2012, **536**, S324-S328.
11. J. Xiao, P. Liu, Y. Liang, H. B. Li and G. W. Yang, *Nanoscale*, 2013, **5**, 899-903.
12. J. Nelayah, N. T. Nguyen, D. Alloyeau, G. Y. Wang and C. Ricolleau, *Nanoscale*, 2014, **6**, 10423-10430.
13. W. W. Xu, X. Y. Song, N. D. Lu and C. Huang, *Acta Mater.*, 2010, **58**, 396-407.
14. W. W. Xu, X. Y. Song, N. D. Lu, M. Seyring and M. Rettenmayr, *Nanoscale*, 2009, **1**, 238-244.
15. Z. X. Zhang, X. Y. Song and W. W. Xu, *Acta Mater.*, 2011, **59**, 1808-1817.
16. Y. Khan and B. Mueller, *Journal of the Less-Common Metals*, 1973, **32**, 39-45.
17. Y. Y. Kostogorova-Beller, M. J. Kramer and J. E. Shield, *J. Mater. Res.*, 2008, **23**, 2886-2896.
18. C. Gammer, C. Mangler, C. Rentenberger and H. P. Karnthaler, *Scr. Mater.*, 2010, **63**, 312-315.
19. W. Coene, P. H. L. Notten, F. Hakkens, R. E. F. Einerhand and J. L. C. Daams, *Philos Mag A*, 1992, **65**, 1485-1502.
20. D. Alloyeau, C. Ricolleau, C. Mottet, T. Oikawa, C. Langlois, Y. Le Bouar, N. Braidy and A. Loiseau, *Nat. Mater.*, 2009, **8**, 940-946.
21. S. Aich and J. E. Shield, *J. Magn. Magn. Mater.*, 2007, **313**, 76-83.
22. M. J. Hytch and M. Gandais, *Philos Mag A*, 1995, **72**, 619-634.
23. M. J. Hytch, *Microsc Microanal M*, 1997, **8**, 41-57.
24. M. Seyring, X. Y. Song, A. Chuvilin, U. Kaiser and M. Rettenmayr, *J. Mater. Res.*, 2009, **24**, 342-346.
25. C. W. T. Bullelieuwma, W. Coene and A. F. Dejong, *Adv. Mater.*, 1991, **3**, 368-378.
26. W. Ostertag and K. J. Strnat, *Acta Crystallographica*, 1966, **21**, 560-&.
27. D. A. Porter and K. E. Easterling, *Phase transformations in metals and alloys*, CRC Press, Boca Raton, Fla., 2004.
28. W. W. Xu, X. Y. Song and Z. X. Zhang, *Appl. Phys. Lett.*, 2010, **97**, 3.
29. X. Y. Song, W. W. Xu and Z. X. Zhang, *Acta Phys. Sin.*, 2012, **61**, 8.
30. R. A. Andrievski, *J. Mater. Sci.*, 2003, **38**, 1367-1375.
31. Q. P. Meng, Y. H. Rong and T. Y. Hsu, *Phys. Rev. B*, 2002, **65**.
32. M. Seyring, X. Y. Song and M. Rettenmayr, *ACS Nano*, 2011, **5**, 2580-2586.